Supplementary Materials for

Theta-Aurora Dynamics: Ionospheric Mapping of Evolving Magnetospheric Plasma Boundaries

Xin-Ming Chen, Zan-Yang Xing*, Qing-He Zhang, Yong-Liang Zhang, Hui-Gen Yang, L. R. Lyons, K. Oksavik, S. E. Milan, Rui-Long Guo, Tong Xu, Bin-Bin Tang, Xiang-Yu Wang, Xiang-Yao Zeng, Yu-Zhang Ma, Yong Wang, Lu Sheng, Duan Zhang, Yanju Sun

*Corresponding author. Email: xingzanyang@sdu.edu.cn

The PDF file includes:

Materials and Methods
Figs. S1 to S5

Other Supplementary Materials for this manuscript include the following:

Movies S1 to S3

Materials and Methods

Method: PPMLR-MHD model

This model is a high-resolution 3D global MHD simulations, and is called Piecewise Parabolic Method with a Lagrangian Remap to MHD (PPMLR-MHD)(*21*), that is driven by IMF conditions and solar wind parameters. This approach is designed especially for the solar wind – magnetosphere – ionosphere coupling processes with a low numerical dissipation in examining possible instabilities inherent(*22–25*). The characteristics of magnetospheric plasma, including velocity, temperature, and density, can be obtained from this MHD model with high temporal and spatial resolutions. The model presents results in a Cartesian coordinate system with the Earth located at the origin. The x-axis points toward the Sun, the y-axis toward the dusk side, and the z-axis toward the north. The magnetic field of earth is approximated using a dipole field with a magnitude of 8.06×10^{22} Am^{-1}.

Input conditions: Specifically, when OMNI observations are available, the MHD model is driven by the measured solar wind and IMF values at those times. When OMNI data are missing, we fill the gap by assigning the most recent preceding time with valid OMNI data to all subsequent time steps until the next valid observation becomes available. In other words, the solar wind parameters are held constant during each data gap, using the last observed values. This approach ensures a continuous input parameters of MHD simulation while remaining strictly consistent with the observations whenever they exist.

Initial conditions: The simulation procedure begins by using the interplanetary magnetic field (IMF) and solar wind parameters at the first time point of the simulation period as the upstream inputs. These conditions are then extended over a period of time. After a prolonged simulation period, the system reaches a quasi-steady state, which is independent of the initial conditions and determined solely by the system parameters, including the ionospheric conductivity and the interplanetary conditions.

Boundary conditions: The numerical box has six outer boundaries, including an inflow boundary at the sunward side (x=30 R_E), symmetry boundaries at the equatorial plane (z=0 R_E) and the noon–midnight meridian (y=0 R_E), and free (outflow) boundaries at x=−300 R_E and y=z=150 R_E. At the inflow boundary, all quantities are specified according to the upstream interplanetary conditions; at the free boundaries, At the free boundaries, all quantities are evaluated by equivalent extrapolation. An inner boundary of radius 3 RE is set for the magnetosphere to avoid the complexities associated with the plasmasphere and large MHD characteristic velocities from the strong magnetic field.

Time steps: The PPMLR-MHD solver advances the solution from t n to t n+1 with time-step length Δ t (t n+1 − t n = Δ t) and has second-order accuracy in time. In this work, Δ t is used as 60s.

Spatial resolution: The size of the numerical box extends from 30 R_E to 100 R_E along the Sun-Earth line and from –50 R_E to 50 R_E in Y and Z directions, with 240 ×240×240 grid points. A uniform near-Earth mesh (0.2 R_E) is used in $-10\ R_E \le x \le 10\ R_E$ and $0\ R_E \le y, z \le 10\ R_E$, and the grid spacing increases outward with a geometric stretching factor of 1.05.

Fig. S1.

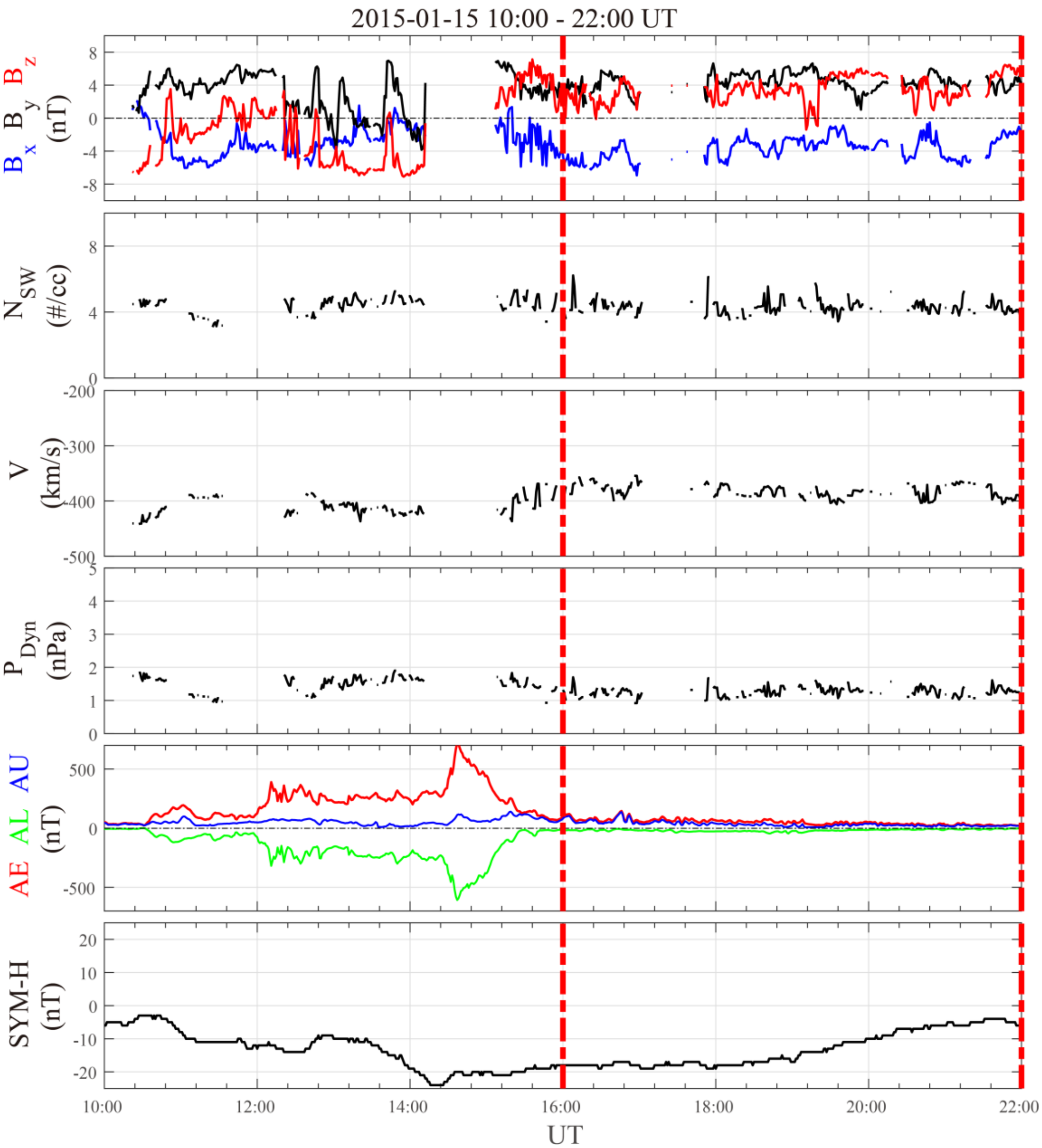

Figure S1. An overview of the solar wind, IMF, and geomagnetic conditions during 1600–2400 UT on 15 January 2015. Parameters shown are: the three IMF components, the solar wind velocity (V), the solar wind, dynamic pressure (PDyn), and the geomagnetic indexes (AU, AE, AL, SYM-H) obtained from the 1 min high-resolution OMNI database. These parameters have been lagged by 7 min to allow for propagation from the bow shock nose to the dayside magnetopause.

Fig. S2.

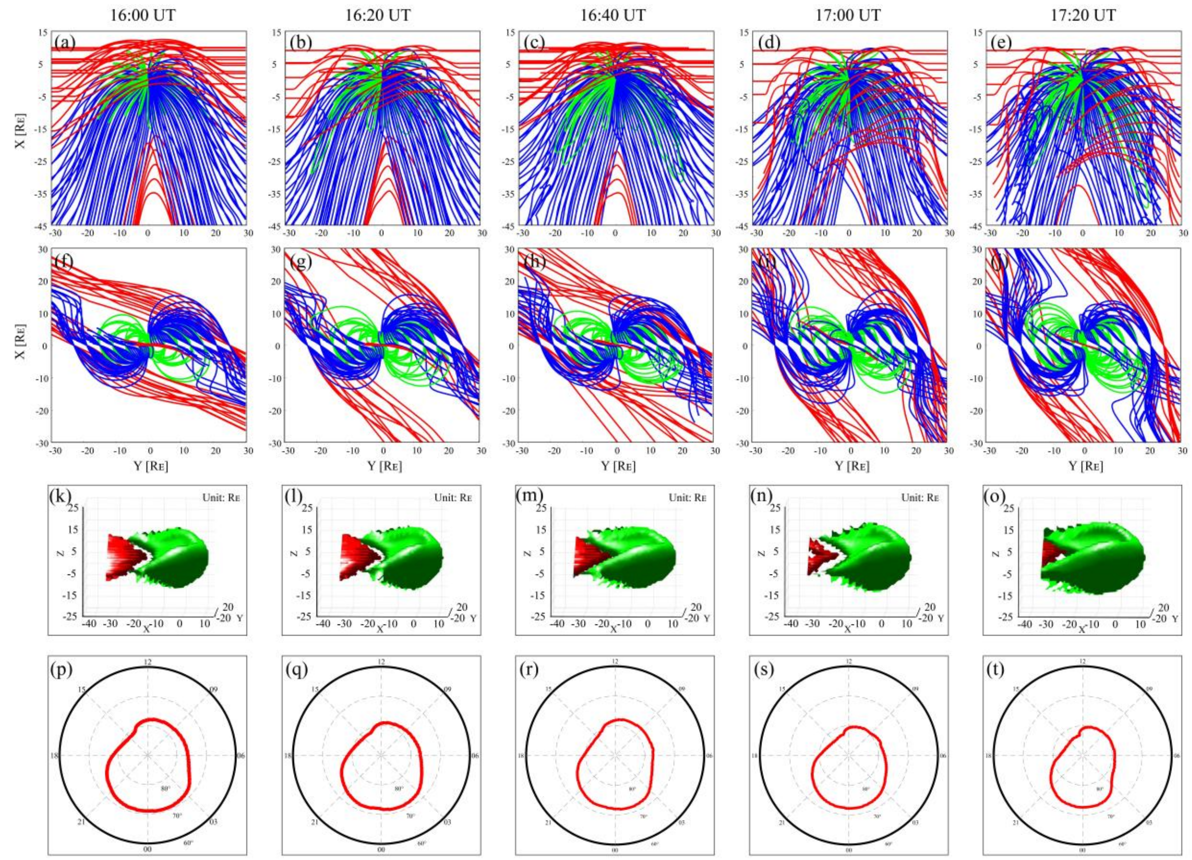

Figure S2. The 2-D results of magnetic field configuration, 3-D field configuration, and the extent of the polar cap region in PPMLR-MHD simulations. a-j show the 2-D results of the magnetic field configuration at five different time steps. The red lines represent completely open magnetic field lines, the blue lines represent semi-open magnetic field lines, and the green line represents completely closed magnetic field lines, which are the observation results from the X-Y and Y-Z planes, respectively. **k-o** display the 3-D results of the magnetic field configuration at five different time steps. The green structures indicate the 3D configuration of closed magnetic field lines, while the red structures represent the open magnetic field line structures in the magnetotail. The gaps between these structures indicate the location of tail reconnection during the event. **p-t** show the extent of the polar cap at five different time steps.

Fig. S3.

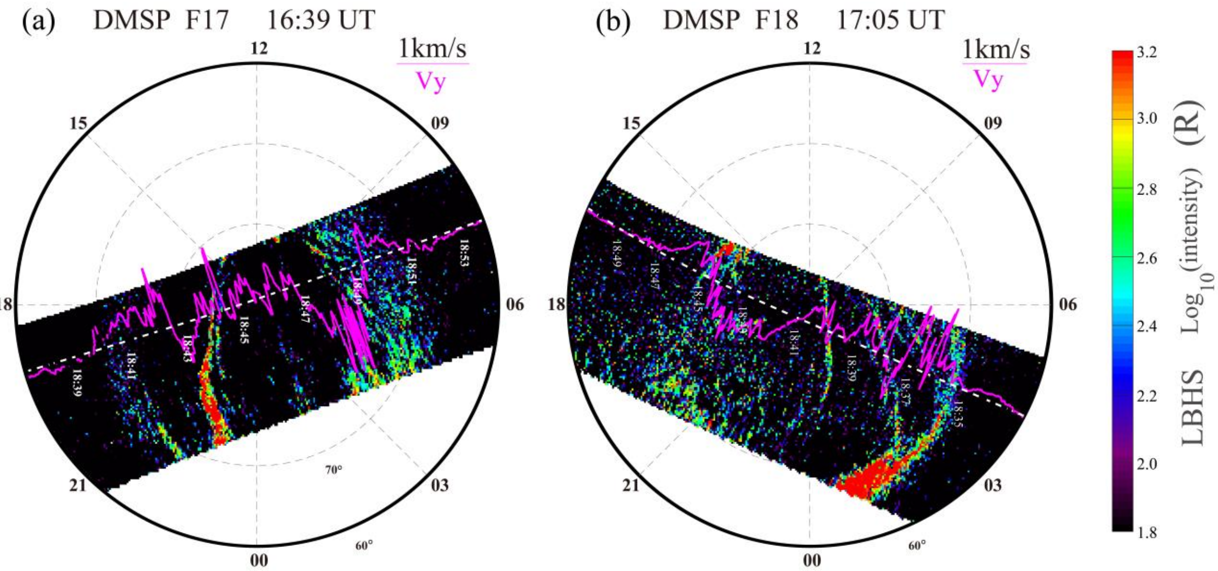

Figure S3. The result of the extent of the polar cap region from T96 model in the Northern Hemisphere. a-b. The red line represents the boundary between open and closed magnetic field lines, overlaid on the DMSP observations. The satellite track (white dashed line) and velocity of cross-track horizontal plasma drift (magenta line) are overlaid. The times corresponding to these results are marked above the image for reference.

Fig. S4.

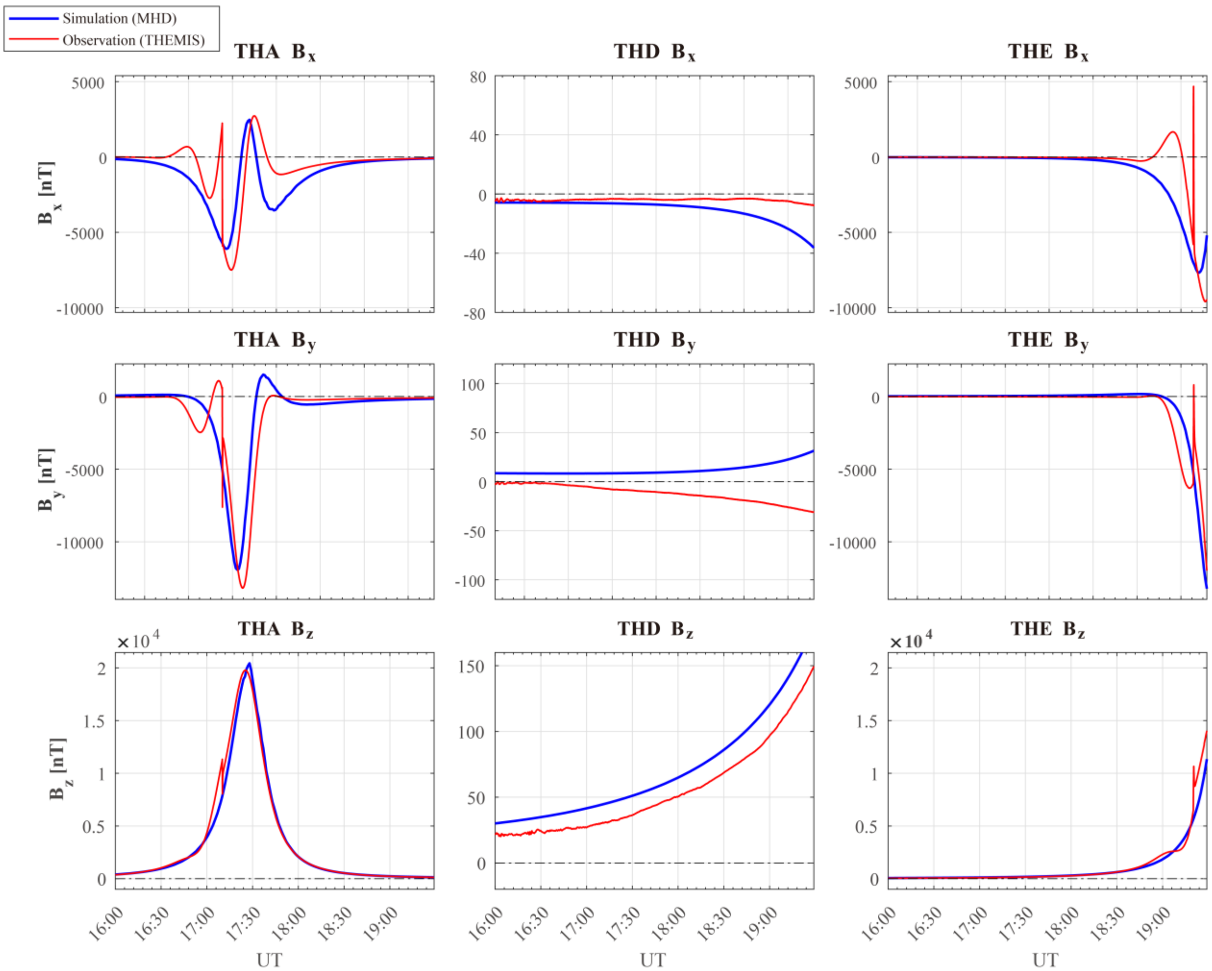

Figure S4: The result of the magnetic field from Themis satellites and MHD simulation. Each row represents one magnetic field component, and each column corresponds to a different spacecraft. The time interval spans from **16:00 UT to 19:30 UT**, showing the evolution of the magnetic field across the event.

Fig. S5.

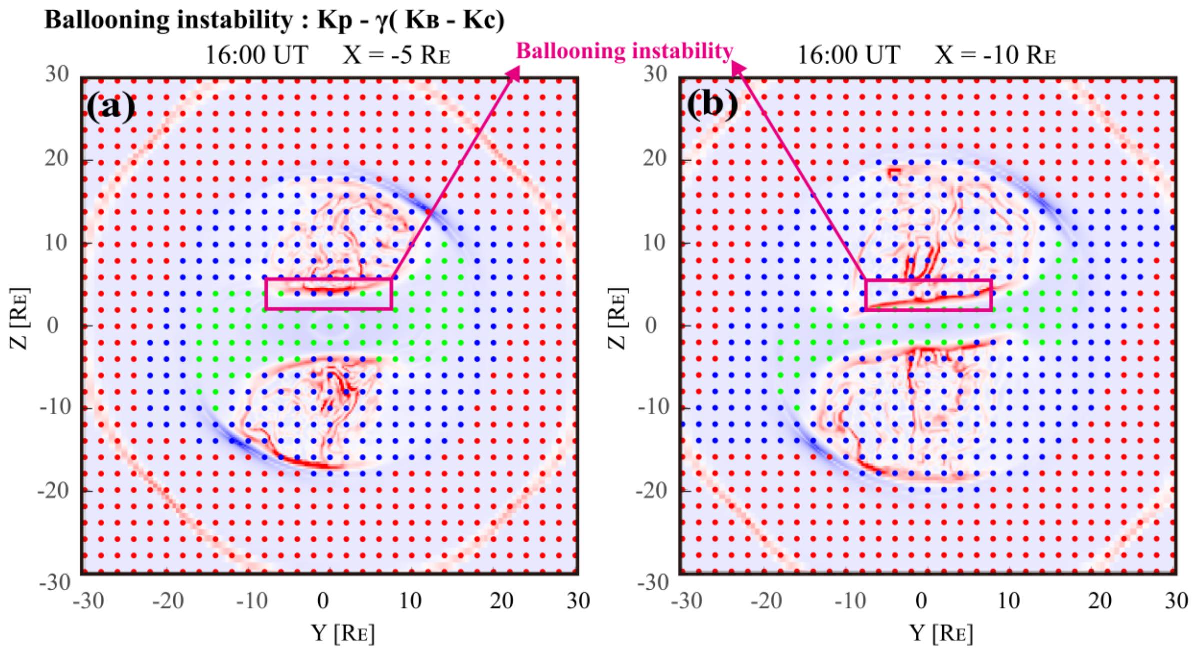

Figure S5. The result of the Ballooning instability from MHD model. a-b. Using MHD simulation, the conditions for ballooning instability are calculated using the formula given in Golovchanskaya et al. (2006), with the opening and closing of closed magnetic field lines superimposed on it. The red border emphasizes the location of the plasma sheet boundary that is conducive to ballooning instability.

Movie S1.

The movie consists of two distinct sections, arranged from top to bottom, each presenting plasma characteristics of the MHD simulation results. The first section depicts the temporal evolution of plasma density distribution in Z=0 plane, with the plasma velocity at each location superimposed at each time frame. The second section showcases the corresponding changes in plasma temperature distribution, with the foot points of the closed magnetic field lines superimposed on it. Both sections cover a time span from 16:00 UT to 18:00 UT.

Movie S2.

The movie consists of two distinct sections, arranged from top to bottom, each presenting plasma characteristics of the MHD simulation results. The first section depicts the temporal evolution of plasma density distribution in Y=6 plane, with the plasma velocity at each location superimposed at each time frame. The second section showcases the corresponding changes in plasma temperature distribution, with the foot points of the closed magnetic field lines superimposed on it. Both sections cover a time span from 16:00 UT to 18:00 UT.

Movie S3.

The movie consists of three distinct sections, arranged from left to right, each presenting plasma characteristics of the MHD simulation results. The first section depicts the temporal evolution of plasma density distribution in X=-20 plane, with the plasma velocity at each location superimposed at each time frame. The second section showcases the corresponding changes in plasma temperature distribution, with the foot points of the closed magnetic field lines superimposed on it. The third section displays the heat flux along the magnetic field lines, where a value greater than 0 indicates that the direction of the heat flux is the same as that of the magnetic field lines. ALL sections cover a time span from 16:00 UT to 18:00 UT.